

Stratification-induced scale splitting in convection

O. V. Shcheritsa^{a,*}, A. V. Getling^b, O. S. Mazhorova^a

^a*Keldysh Institute of Applied Mathematics, Moscow, 125047 Russia*

^b*Skobeltsyn Institute of Nuclear Physics, Lomonosov Moscow State University,
Moscow, 119991 Russia*

Abstract

The coexistence of motions on various scales is a remarkable feature of solar convection, which should be taken into account in analyses of the dynamics of magnetic fields. Therefore, it is important to investigate the factors responsible for the observed multiscale structure of solar convection. In this study, an attempt is made to understand how the scales of convective motions are affected by the particularities of the static temperature stratification of a fluid layer. To this end, simple models are considered. The equations of two-dimensional thermal convection are solved numerically for a plane horizontal fluid layer heated from below, in an extended Boussinesq approximation that admits thermal-diffusivity variations. These variations specify the stratification of the layer. The static temperature gradient in a thin sublayer near the upper surface of the layer is assumed to be many times larger than in the remainder of the layer. In some cases, distributed heat sinks are assumed to produce a stably stratified region overlying the convective layer. Manifestations of the scale-splitting effect are noted, which depend on the boundary conditions and stratification; it becomes more pronounced with the increase of the Rayleigh number. Small-scale convection cells are advected by larger-scale flows. In particular, the phase trajectories of fluid particles indicate the presence of complex attractors, which reflect the multiscale structure of the flow. The effect of the stably stratified upper sublayer on the flow scales is also considered.

Keywords:

multiscale convection; temperature stratification

1. Introduction

The dynamics of solar magnetic fields depends crucially on the structure of the velocity field in the convection zone. In particular, the coexistence of convective motions on various scales is clearly reflected by the magnetic-field structure on the photospheric levels.

At least four types of cellular structures, strongly differing in their scale, can be identified with certainty on the solar surface and attributed to the phenomenon of thermal convection, viz., granules, mesogranules, supergranules and giant cells. This multiscale structure is an important feature of solar convection, which should be taken into account in studying the dynamics of

*Corresponding author

Email addresses: shchery@mail.ru (O. V. Shcheritsa), A.Getling@mail.ru (A. V. Getling), olgamazhor@mail.ru (O. S. Mazhorova)

magnetic fields. It has not yet received a convincing explanation, and an adequate hydrodynamic description must be given to both the spatial structure of the flows and the factors responsible for its development.

It can naturally be expected that, if convection cells are not large in their plan size compared to the full thickness of the convecting fluid layer, they should also be vertically localised (“suspended”) in a relatively thin portion of this layer. This is obviously possible if a certain sublayer (height interval) with a convectively unstable thermal stratification is contiguous with another sublayer where the stratification is stable and exerts a braking action on the convective motion. In this case, the flow nevertheless penetrates into the stable region — penetrative convection occurs. If, however, the entire layer (from top to bottom) is convectively unstable, the possibility for motion being localised in a relatively thin sublayer is not so trivial. Such localisation can most easily be achieved by introducing, e.g., sufficiently strong temperature variations of viscosity (see, e.g., Stengel et al., 1982). At the same time, similar effects of other factors remain little explored. Even less obvious is the coexistence of small cells with larger ones, filling the entire layer thickness. Such coexistence will here be referred to as the scale-splitting effect.

Quite likely, scale splitting could result from sharp changes in the static vertical entropy gradient (or the static temperature gradient in the case of an incompressible fluid) at some heights. Under the conditions of the solar convection zone, there are some prerequisites for this effect, traditionally attributed to the enhanced instability of the sublayers of partial ionisation of hydrogen and helium. In these sublayers, the specific heat of the plasma is increased and the adiabatic temperature gradient accordingly decreased, while the radiative gradient is increased. This idea was put forward by Simon & Leighton (1964) in the context of the observed coexistence of granulation and supergranulation and then extended to mesogranulation by November et al. (1981). It is typically assumed that the zones of partial ionisation of neutral hydrogen, neutral helium and singly ionised helium control the formation of granules, mesogranules and supergranules, respectively. The depths of location of these zones are suggested to determine the characteristic sizes of these three sorts of convection cells. The latter conjecture is, however, fairly arbitrary from the standpoint of the theory of convection, as we shall see below.

On the other hand, stratification effects are not the sole candidate for the scale-splitting mechanism. Solar convection is violent, turbulent fluid motion with a complex spectrum, and hydrodynamic instabilities of some larger-scale motion can produce secondary, smaller-scale flows. Conversely, Brummell et al. (1995) note possible self-organisation processes in turbulence (inverse energy cascades), which can give rise to coherent structures. Cattaneo et al. (2001) attribute the formation of mesogranules to the collective interaction between the granules, leaving the effects of stratifications beyond the scope of their study.

Although the structure of solar convection has long been explored using numerical simulations, the scale-splitting effect has not yet received a convincing explanation. In particular, DeRosa et al. (2002) simulate convection in a thin shell and note the presence of various scales in the velocity field; however, the large-scale flows computed in that study are associated with global processes, while the size of the smaller cells is controlled by the thickness of the shell. These cells are not “suspended” near the outer boundary of the shell. Kitiashvili et al. (2012) investigate the multiscale flow dynamics of vortical structures but do not reveal cellular structures.

Previously, Getling (1976, 1980) considered linear problems on convection in layers with near-surface jumps in the static temperature gradient, from low values in the bulk to high values in a boundary sublayer. Such a jump was regarded as a model representation of the sharp jump in the entropy gradient at depths of order 1 Mm below the solar photosphere. In the framework of the model, indirect indications for scale splitting were found. These expectations were substantiated

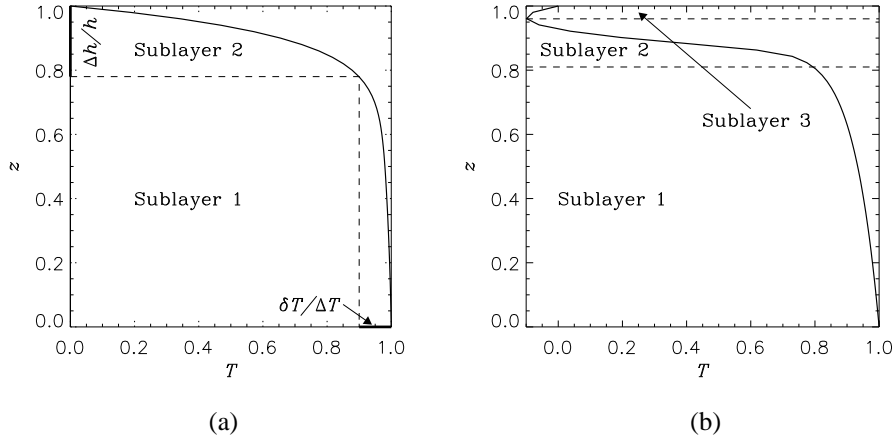


Figure 1: Static temperature profiles (in dimensionless variables): (a) monotonic profile for $a = 5$, $b = 600$, $n = 10$; (b) nonmonotonic profile for $a = 0.01$, $b = 600$, $n = 10$, $q_0 = -2$, $z_0 = 0.8$

in part by nonlinear numerical computations (Getling & Tikhomolov, 2007). It proved, however, that the tendency for convection cells to fill the whole layer thickness is very strong, and small-scale, near-surface convective motions develop only if the jump is very sharp and the high-gradient sublayer is very thin.

We investigate here possibilities of scale splitting by means of numerically simulating two-dimensional convective flows in the framework of similar simple models. Although two-dimensional simulations have only limited applicability to natural fluid-dynamic systems, they are still of some interest, being fairly simple and well tractable (Schmalzl et al., 2004); simulations of two-dimensional turbulent convection in a density-stratified fluid layer by Rogers et al. (2003) can be mentioned as an example. Our simplified formulation of the problem appears to be useful from the standpoint of evaluating the role of some factors, taken alone, among those controlling the static thermal stratification of the layer.

2. Formulation of the problem and numerical technique

Assume that a plane horizontal layer $0 < z < h$ of a viscous, incompressible fluid is heated from below and consider its finite segment $0 < x < L$ in which we shall simulate two-dimensional ($\partial/\partial y = 0$) convection flows. Let the bottom and top boundaries be perfect thermal conductors and let their temperatures be constant and equal to $T_{\text{bot}} = \Delta T > 0$ and $T_{\text{top}} = 0$, respectively. We also assume that the sidewalls of the region are thermally insulated. The no-slip impermeability conditions are specified at the bottom and side boundaries of the domain. The top boundary may be either rigid (no-slip) or stress-free.

We are interested in situations where the static temperature varies little (by $\delta T \ll \Delta T$) across the main portion of the layer, of thickness $h - \Delta h$, $\Delta h \ll h$ (Sublayer 1), while the most part of the temperature difference, $\Delta T - \delta T$, corresponds to Sublayer 2 with a small thickness Δh , near the upper surface (Fig. 1). The kink near $z = h - \Delta h$ in the temperature profile specified in this way qualitatively resembles the transition (above depths of order 1 Mm) from the bulk of the solar convection zone, where the stratification is weakly superadiabatic, to the strongly

unstable subphotospheric layers. To obtain such profiles, we assume the thermal diffusivity to be temperature-dependent:

$$\chi(T) = 1 + aT + bT^n. \quad (1)$$

In some cases, we introduce heat sinks uniformly distributed over the region above a certain level $z = z_0$ located in Sublayer 2 to obtain temperature profiles with a minimum at a certain height, so that a stable Sublayer 3 be located above Sublayer 2 (see below). This sublayer is considered to play the role of a “soft boundary,” or “penetrable lid,” as do the stable layers located immediately above the temperature minimum in the solar atmosphere. We shall give no attention to the flow structure within this sublayer.

To describe the dynamics of convection, we use an extended Boussinesq approximation, which admits thermal-diffusivity variations (for a discussion of different versions of the Boussinesq approximation, see, e.g., Getling, 1998). If the layer thickness h is chosen as the unit length, ΔT as the unit temperature and the characteristic time of viscous momentum transport, $\tau_v = h^2/\nu$, as the unit time (ν being the kinematic viscosity), the governing equations assume the following dimensionless form:

$$\frac{\partial \mathbf{v}}{\partial t} + (\mathbf{v} \cdot \nabla) \mathbf{v} = -\nabla \varpi + \hat{\mathbf{z}} \frac{R}{P} (T - T_s) + \Delta \mathbf{v}, \quad (2)$$

$$\frac{\partial T}{\partial t} + \mathbf{v} \cdot \nabla T = \frac{1}{P} \nabla \cdot \frac{\chi(T)}{\chi(T_{\text{top}})} \nabla T, \quad (3)$$

$$\nabla \cdot \mathbf{v} = 0; \quad (4)$$

here, $\hat{\mathbf{z}}$ is the z -directed unit vector, $T_s(z)$ is the static temperature distribution, $\chi(T)$ is the thermal diffusivity, ϖ is the nondimensionalised pressure and

$$R = \frac{\alpha g \Delta T h^3}{\nu \chi(T_{\text{top}})} \quad \text{and} \quad P = \frac{\nu}{\chi(T_{\text{top}})}$$

are the Rayleigh and Prandtl numbers, α being the volumetric coefficient of thermal expansion of the fluid and g the gravitational acceleration.

For two-dimensional incompressible flows, the stream function ψ and vorticity ω specified by the equations

$$v_x = \frac{\partial \psi}{\partial z}, \quad v_z = -\frac{\partial \psi}{\partial x}, \quad \omega = -\left(\frac{\partial^2 \psi}{\partial x^2} + \frac{\partial^2 \psi}{\partial z^2} \right)$$

are variables convenient for constructing a computational algorithm. We solve equations (2)–(4) with properly chosen boundary conditions using the standard procedure of splitting physical processes (Kovenya & Yanenko, 1981). Specifically, we first employ a matrix algorithm (Mazhorova & Popov, 1980, 1981) to determine the velocity field from (2) written in terms of ψ and ω ; next, we find the temperature distribution in the layer from (3). We use a conservative scheme of the second-order accuracy in the spatial coordinates and of the first-order accuracy in time (Arakawa, 1966). Calculations are carried out on a nonuniform grid, which is finer near the top and bottom layer boundaries. The horizontal size of our computational domain is $L = 5\pi h = 15.7h$, and the total number of nodes is 1024×51 .

Most calculations were done for static temperature profiles specified by dependences (1) with $a = 5 - 20$, $b = 600$, $n = 10 - 80$, the temperature varying monotonically in these cases (Fig. 1a).

Alternatively, nonmonotonic profiles (Fig. 1b) were obtained by specifying heat sinks uniformly distributed with a density $-q$ (i.e., heat sources with a negative density q) above the height z_0 , as the solution of the problem

$$\frac{\partial}{\partial z} \left(\chi(T) \frac{\partial T}{\partial z} \right) + q = 0, \quad q = \begin{cases} q_0 < 0, & z > z_0 \\ 0, & z < z_0 \end{cases}.$$

For the sake of comparisons, we also considered the case where the static temperature profile of the form shown in Fig. 1a was produced by specially chosen temperature-dependent heat sources, with a constant thermal diffusivity (1). The results differ substantially from those obtained for the case of the temperature-dependent thermal diffusivity, which therefore appears to be physically more appropriate in the context of solar convection.

In our simulations, the flow is initiated by introducing random thermal perturbations at a certain height within the upper sublayer.

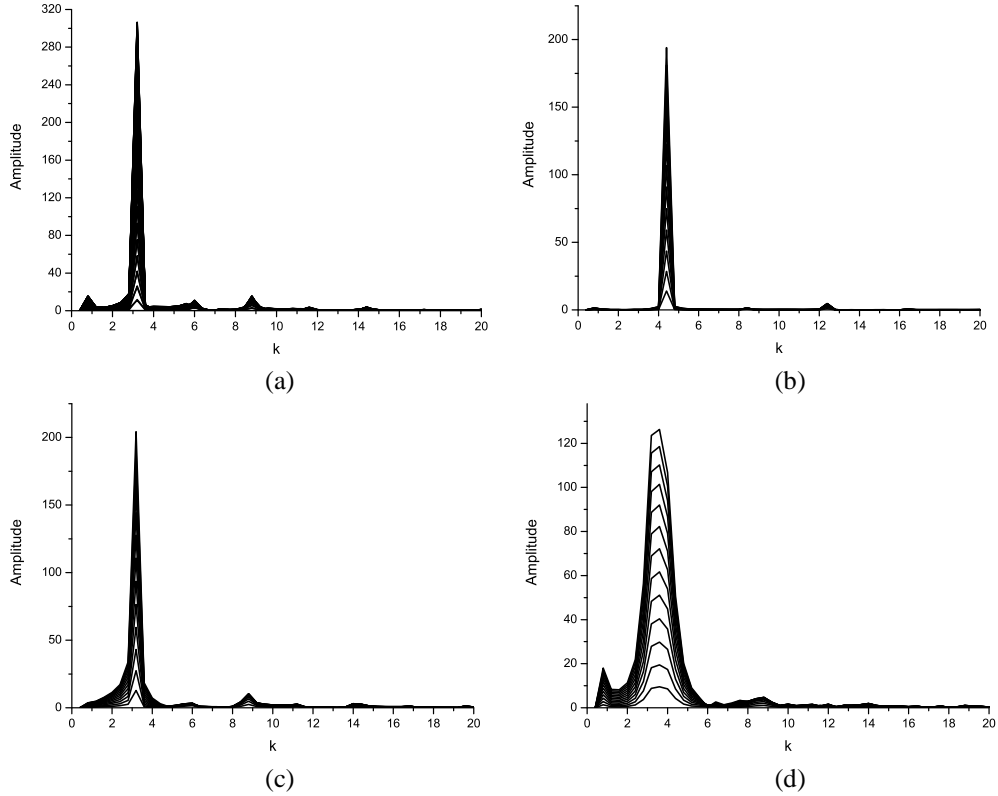


Figure 2: Fourier spectra of simulated convective flows ($a = 5$, $b = 600$, $n = 10$; different curves in the same graph correspond to different heights z): (a) rigid upper boundary, $R = 10R_c$ ($R_c = 1.95 \times 10^6$); (b) free upper boundary, $R = 10R_c$ ($R_c = 1.8 \times 10^6$); (c) rigid upper boundary, $R = 55R_c$ ($R_c = 1.95 \times 10^6$); (d) free upper boundary $R = 55R_c$ ($R_c = 1.8 \times 10^6$).

3. Simulation results

3.1. Monotonic static temperature profiles

Some preliminary results of our simulations were reported by Getling et al. (2013). Here, we substantially extend the explored region of parameter space (in particular, to higher Rayleigh numbers) and discuss the results more comprehensively. In particular, along with the Fourier transform, we use the technique of phase trajectories of fluid particles to analyse the flow structure.

For both the no-slip and stress-free boundary conditions at the upper surface of the layer, the critical Rayleigh number R_c was determined in the process of simulation. In the regimes studied, it lies in the range, roughly, $R_c = 1.95 \times 10^6$ – 3.8×10^6 (depending on a , b and n) for a rigid upper boundary and $R_c = 4 \times 10^5$ – 1.8×10^6 for a free upper boundary; the Prandtl number in our calculations is $P = 1$. We present here our simulations for two degrees of supercriticality, $R = 10R_c$ and $R = 55.5R_c$. The qualitative features of the results turn out to be little sensitive to the choice of parameters a and n in the above-mentioned ranges.

We analyse the flow structure using the discrete Fourier transform of the stream function with respect to the horizontal coordinate x at given heights z . High-frequency harmonics are present in the spectrum, whose amplitudes amount to 5–16% of the amplitude of the fundamental mode, depending on the parameters of the problem (Fig. 2). To separate the small-scale component of the velocity field and visualise the fine cellular structures present in the flow, we use an ideal low-pass filter (Blahut, 1985) and subtract the obtained large-scale component from the original field. This procedure proved to be efficient in the case of the rigid upper boundary (Figs 3, 4). In the case of the free upper boundary, however, the more complex appearance of the spectra made our attempts of filtering unsuccessful.

If the upper horizontal boundary is rigid, motion starts developing as small-scale convection in Sublayer 2. Later, the disturbances penetrate deeper and gradually involve the entire layer depth. As a result, large-scale convection rolls emerge, with a width of about the layer thickness. As this takes place, the small-scale flow in the upper sublayer does not disappear and assumes the form of smaller rolls with a size typically exceeding the sublayer thickness. A flow of a similar small scale also develops near the bottom layer boundary. It should be noted that, if the temperature profile is linear (the classical Rayleigh–Bénard problem), simulations at the same R and P do not reveal small-scale structures. In moderately supercritical regimes, the small rolls are especially pronounced above and below the contact sections of large rolls. As the Rayleigh number is increased, the small rolls occupy a progressively wider region, and a tendency to the formation of two layers of small-scale rolls is observed. Thus, in the fluid layer stratified on the whole unstably, large convection cells¹ filling the entire layer depth coexist with smaller ones localised in relatively thin sublayers (Figs 3, 4). The scale-splitting effect is more pronounced at higher Rayleigh numbers: the near-surface cells singled out by subtracting the large-cell flow are smaller and more clear-cut at $R = 55.5R_c$ (Fig. 4) than at $R = 10R_c$ (Fig. 3). It is worth noting that their location is not directly controlled by the thickness sublayer of the large static temperature gradient (Sublayer 2 in Fig. 1a).

In the case of a free upper boundary, the flow also originates in the upper sublayer, after which the emerged small-scale structures penetrate deeper into the layer, stimulating the formation of a flow throughout the layer. The cells in Sublayer 1 tend to grow in size; however, the small-scale

¹ By a convection cell in a two-dimensional flow, a pair of neighbouring rolls is meant.

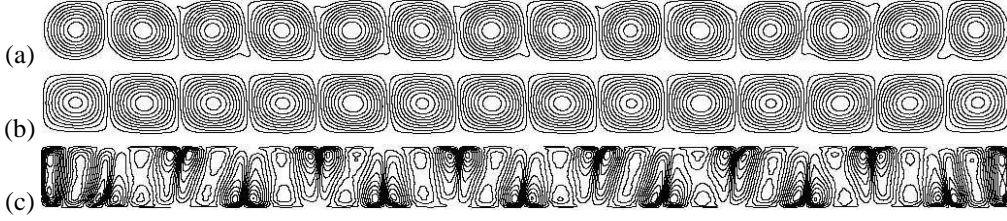


Figure 3: Convective flow computed for a rigid upper boundary and $R = 10R_c$ ($R_c = 1.95 \times 10^6$), $P = 1$, $a = 5$, $b = 600$, $n = 10$, with large cells and a smaller-scale flow coexisting: (a) streamlines (contours of the stream function); (b) large-scale structures separated from the flow using an ideal low-pass filter; (c) small-scale structures obtained by subtracting the large-scale component from the full stream-function field. This flow pattern does not undergo qualitative changes after $t \sim 0.1$, remaining weakly time-dependent (we recall that the time is measured in the units of the time of viscous momentum transport, τ_V).

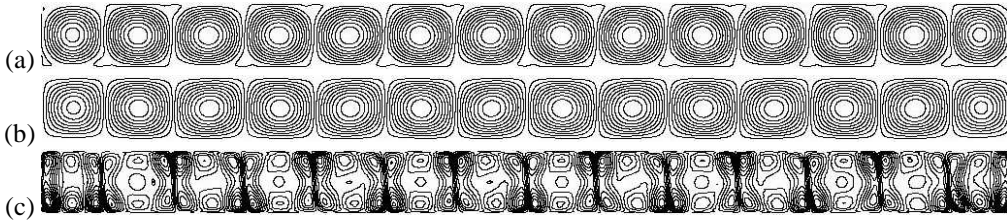


Figure 4: Same as in Fig. 3 but for $R = 55.5R_c$. This pattern has been formed by $t \sim 0.05$ and does not undergo qualitative changes at later times, although is not quite stationary.

structures present in Sublayer 2 control this process: as the horizontal size of a large structure becomes considerably larger than the layer thickness, the cells moving down from the upper sublayer break this structure into two portions (Figs 5, 6). In contrast to the case of a rigid upper boundary, where the number of large rolls is constant, the number of large-scale structures now varies between 10 and 15.

The spectrum of the flow (Figs 2b, d) is now more complex than in the case of the rigid upper boundary (Figs 2a, c). Since the number of large structures is variable, the fundamental mode is also time-dependent. Harmonics with different wavenumbers dominate in the bulk of the layer and in the upper sublayer. The enhancement of the small-scale component frequently parallels with the weakening of the large-scale component, and vice versa — a sort of intermittency is observed. As this takes place, the sublayers in which the cells are localised vary in their thickness and do not coincide with the sublayers specified by the static vertical temperature profile. In contrast to the case of a rigid upper boundary, the small-scale structures are localised only in the upper part of the layer.

If the profile shown in Fig. 1a is produced by a heat-source distribution, the flow behaves in a very complex manner and has a wide-band spectrum. Although the flow dynamics deserves a careful analysis in this case, it does not appear to be quite relevant to our subject. We plan to present such an analysis elsewhere.

3.2. Nonmonotonic static temperature profile

The nonmonotonic static temperature profile shown in Fig. 1b was created by combining a temperature-dependent thermal diffusivity with distributed heat sinks. The needed profiles were

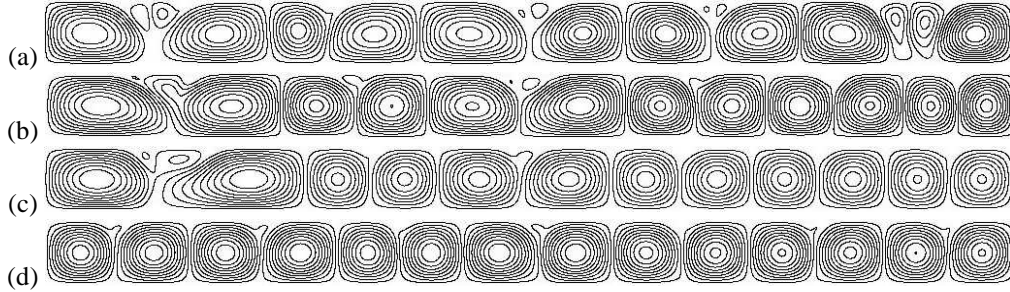


Figure 5: Flow evolution in the case of a free upper boundary, at $R = 10R_c$ ($R_c = 1.8 \times 10^6$), $P = 1$, $a = 5$, $b = 600$, $n = 10$. Streamlines (contours of the stream function) are shown for different times: (a) $t = 0.04$, small-scale cells originating near the upper surface of the layer; (b) $t = 0.045$, the “breaking” effect of the small cells, penetrating into the layer depth, on those large rolls whose horizontal size considerably exceeds the scale optimum; (c) $t = 0.14$, the flow structure formed in the process of penetration of small cells deeper into the layer; (d) $t = 0.22$, a tendency toward the expansion of large-scale cells. The emergence and development of small-scale structures in the upper sublayer. The flow pattern does not undergo qualitative changes at later times.

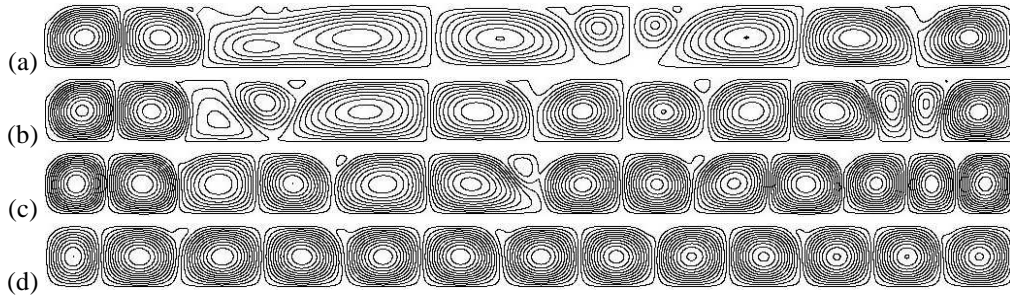


Figure 6: Same as in Fig. 5 but for $R = 55R_c$ and (a) $t = 0.006$, (b) $t = 0.007$, (c) $t = 0.008$ and (d) $t = 0.076$. The flow pattern does not undergo qualitative changes at later times.

obtained at the following parameters: $a = 0.01-0.1$, $b = 600$, $n = 10-20$, $q_0 = -2$, $z_0 = 0.8$. In the regimes studied, the Rayleigh number varied in the range $R = 20\,000-200\,000$ and the Prandtl number was $P = 1$.

The flows computed for the nonmonotonic profile are much less ordered than in the case of the rigid or free upper boundary. They are highly changeable, characterised by permanently arising descending and ascending plumes, and can on the whole be assigned to fairly developed turbulence.

Convection was initiated by introducing a random perturbation of the static temperature profile at a certain height. The dynamics of the flow is highly sensitive to where the initial perturbations are introduced. For this reason, special efforts are required to determine the critical Rayleigh number. At this stage, our very crude estimates based on the simulated regimes near the threshold of convective instability yielded $R_c \approx 13\,000$.

Motion starts developing at the interface between Sublayers 2 and 3, after which small-scale structures penetrate to deeper levels and stimulate the development of the flow in the bulk of the layer (see Fig. 7 and especially Fig. 8). Large-scale structures form, with a vertical size comparable with the layer thickness and horizontal sizes exceeding it. The number of large structures varies in the evolving flow pattern. Fresh small-scale structures permanently originate

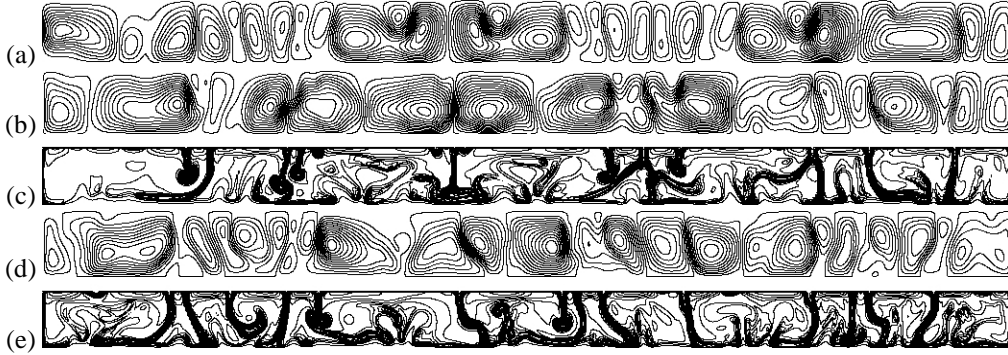


Figure 7: Flow structure in the case of the nonmonotonic static temperature profile, for $R = 20000 \approx 1.5R_c$, $P = 1$ and different times: (a) stream function at $t = 0.21$, small-scale structures penetrate deep into the layer; (b) stream function at $t = 0.42$, developing small-scale structures either glide deep into the layer or break a large structure into two parts; (c) temperature distribution at $t = 0.42$ with local overheat and underheat zones present in the bulk of the layer; (d) stream function at $t = 0.7$, small-scale structures are transferred by the large ones; (e) temperature distribution at $t = 0.7$ with local overheat and underheat zones present in the bulk of the layer. The flow pattern does not undergo qualitative changes at later times.

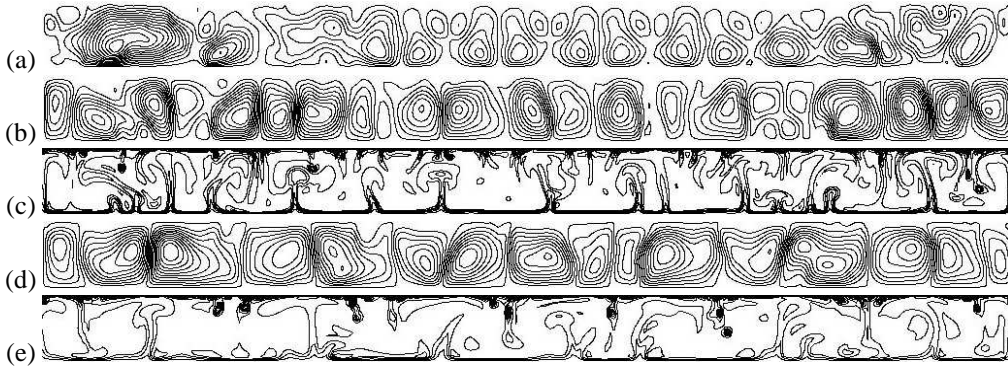


Figure 8: Same as in Fig. heat but for $R = 200000 \approx 15R_c$, $P = 1$ and (a) $t = 0.12$, (b, c) $t = 0.32$, (d, e) $t = 0.8$. The flow pattern does not undergo qualitative changes at later times.

at the interface between the sublayers and either glide deeper between two large structures or break a large structure into two parts, preventing it from increasing its horizontal size (Figs 7b, 8b). In the bulk of the layer, local overheat or underheat zones emerge (see Figs 7c, 7e and also Figs 8c, 8e, where they are more pronounced).

It can be seen from the Fourier transform of the stream function (not presented here) that three or four modes (harmonics) with incommensurate wavenumbers dominate in the spectrum of a well-developed flow. Different modes dominate at different times, so that determining the number of spatial scales present is not a simple task. Applying numerical-homology techniques to the velocity field (Krishan et al., 2007) confirms the coexistence of several spatial scales although does not enable us to determine the size and localisation of the structures.

3.3. Phase space and attractors

The complex structures developing in various flows cannot always be classified and analysed using Fourier-transform-based methods. To make the presence of various flow scales more apparent, we constructed the trajectories of fluid particles in an appropriately defined phase space, (z, v_z) . Several hundred particles differing in their initial position were used. In their motion, all these particles repeatedly passed from one structure to another, and transitions between large structures and between a large and a small structure — possibly with a subsequent return to the large structure — could take place.

If the static temperature profile is monotonic, an attractor can be detected whose structure clearly demonstrates the presence of different flow scales. In Fig. 9a, which refers to the case of a rigid upper boundary, the trajectory of only one particle is shown, others being quite similar. The velocity vanishes near the upper and lower boundaries ($z = 0$ and $z = 1$) according to the no-slip condition, and a passage of the trajectory from the positive to negative half-plane reflects a transition from ascending to descending motion. Therefore, the large ellipses correspond to the large structure and the small ellipses near $z = 0$ and $z = 1$ represent the small-scale flows near the upper and lower boundaries. If the upper boundary is free, small-scale motions are localised only near this boundary (Fig. 9b).

It can be found from Fig. 9a that, for $R = 10R_c$ and the rigid upper boundary, the vertical size of the large structures is equal to the layer thickness h , the size of the small structure being $0.18h$ near the lower boundary and $0.14h$ near the upper boundary. Different scales of the small structures can be due to different thermal diffusivities near $z = 0$ and $z = 1$: $\chi(T_{\text{bot}}) = 605$, while $\chi(T_{\text{top}}) = 1$. In the case of $R = 55R_c$, the size of the small structures is $0.17h$ near the lower boundary and $0.11h$ near the upper boundary (Fig. 9c). If the upper boundary is free, the vertical size of the small structures is $0.18h$ at $R = 10R_c$ (Fig. 9b) and $0.11h$ at $R = 55R_c$ (Fig. 9d).

Similar analyses were done for the case of the nonmonotonic static temperature profile. Various features in the obtained trajectories can be seen in Fig. 10. The closed (or nearly closed) loops of the trajectories located near $z = 0$ or $z = 1$ (Figs 10a, 10c, 10d) evidence the presence of small-scale structures near the lower or the upper layer boundary. The trajectories exemplified in Fig. 10b, 10d indicate the presence of small-scale structures in the bulk of the layer. Thus, the coexistence of large-scale and small-scale cells can be revealed in the problem with a nonmonotonic static temperature profile, and the small-scale structures are distributed over the whole layer thickness rather than localised in thin sublayers. They move through the layer, being advected by the large-scale flow. It should be noted that the spatial trajectories of the particles have numerous nearly horizontal segments, which is reflected by the discontinuities of the phase trajectories seen in Fig. 10.

4. Conclusion

We see that the stratification due to the variable thermal diffusivity, with a sharp kink in the static temperature profile, can give rise to the development of small-scale flows superposed onto larger-scale flows, i.e., on the whole, to the splitting of convection scales. In the case of two rigid boundaries, small-scale cells are localised in both the upper and bottom boundary sublayers. However, small-scale cells are observed only near the upper boundary if it is free. In both cases, the thickness of the localisation zones of small-scale cells does not coincide with the thickness of the sublayer with the sharp temperature change, Δh , and declines with the Rayleigh number increasing. The small-scale structures become more clear-cut at higher Rayleigh numbers. Small

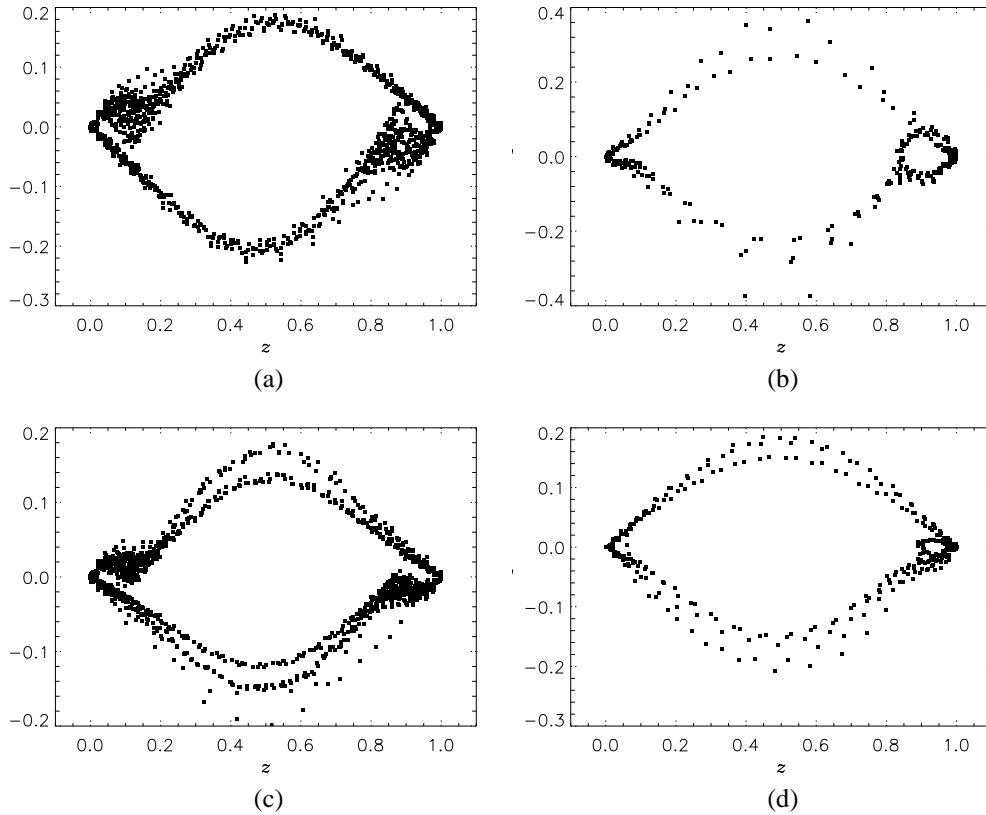


Figure 9: Phase trajectories of a particle in space (z, v_z) ; $a = 5$, $b = 600$, $n = 1$: (a) rigid upper boundary, $R = 10R_c$ ($R_c = 1.95 \times 10^6$); (b) free upper boundary, $R = 10R_c$ ($R_c = 1.8 \times 10^6$), (c) rigid upper boundary, $R = 55R_c$ ($R_c = 1.95 \times 10^6$); (d) free upper boundary, $R = 55R_c$ ($R_c = 1.95 \times 10^6$).

cells are advected by large-scale flows; if the upper boundary is free, this process appears as the sinking of small cells.

The flows computed for the nonmonotonic profile are much less ordered than in the case of the rigid or free upper boundary. They are highly changeable, characterised by permanently arising descending and ascending plumes, and can on the whole be assigned to fairly developed turbulence.

The appearance of phase trajectories in the case of the nonmonotonic profile also counts in favour of the small-scale structures being transferred by the large-scale flow. It is worth noting in this context that, as some observational data suggest, granules are advected by larger-scale flows in the solar convection zone. Analyses of correlations between the brightness variations at two points located not far from each other suggest that granules may even repeatedly emerge on the solar surface, playing a relatively passive role in the convection dynamics (Getling, 2006).

Clearly, the simplified models considered here cannot offer a realistic description of solar convection, the structure of which depends on a multitude of factors, such as the density difference across the convection zone, the complex thermal stratification, the complex equation of

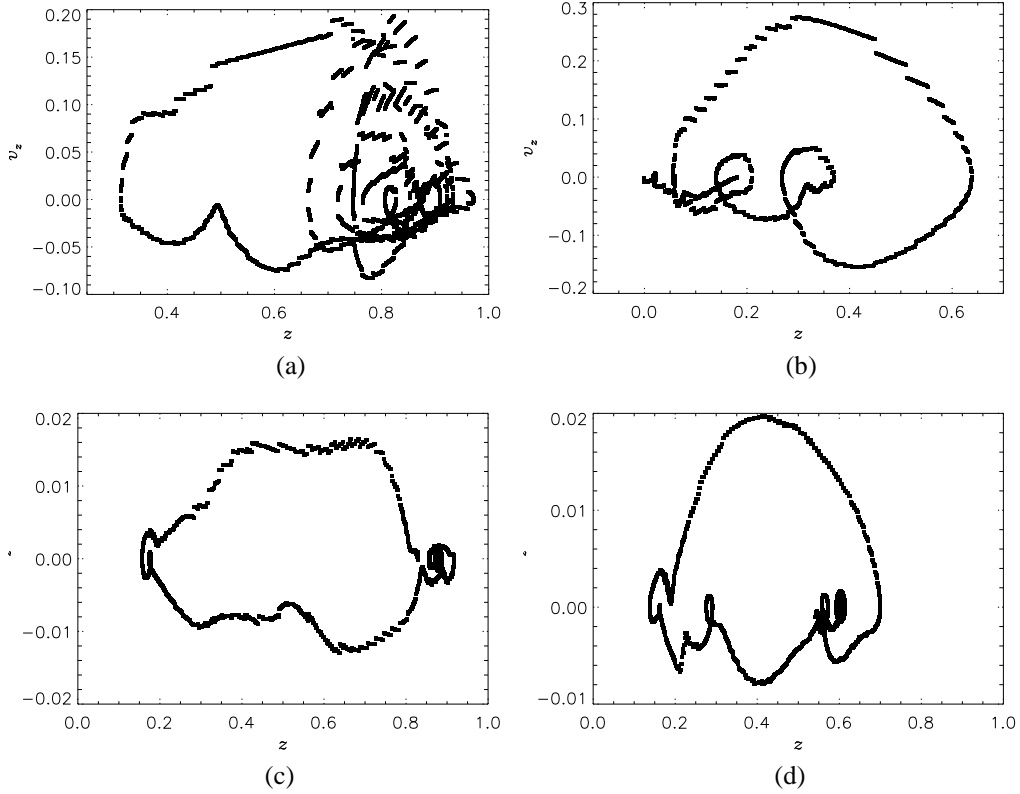


Figure 10: Phase trajectories of different fluid particles in the problem with a nonmonotonic static temperature profile, $\alpha = 0.01$, $b = 600$, $n = 10$: (a, b) $R = 20\,000 \approx 1.5R_c$; (c, d) $R = 200\,000 \approx 15R_c$.

state of the matter (related to the variable ionization degree), radiative heat exchange, etc. Nevertheless, such models are instructive in terms of evaluating the possible role of various factors in the formation of the real pattern.

Acknowledgement

We are grateful to the referees for their constructive criticism and helpful suggestions.

References

- Arakawa, A., Computational design for long-term numerical integration of the equations of fluid motion: Two-dimensional incompressible flow. Part I, *J. Comput. Phys.*, 1, 119-143, 1966; reprinted: 135, 103-114 (CP975697), 1997.
- Blahut, R.E., *Fast Algorithms for Signal Processing*, Addison-Wesley, Boston, 1985.
- Brummell, N., Cattaneo, F., & Toomre, J., Turbulent dynamics in the solar convection zone, *Science*, 269, 1370-1379, 1995.
- Cattaneo, F., Lenz, D., & Weiss, N., On the origin of the solar mesogranulation, *Astrophys. J.*, 563, L91-L94, 2001.

- DeRosa, M.L., Gilman, P.A., & Toomre, J., Solar multiscale convection and rotation gradients studied in shallow spherical shells, *Astrophys. J.*, 581, 1356–1374, 2002.
- Getling, A.V., Convective motion concentration at the boundaries of a horizontal fluid layer with inhomogeneous unstable temperature gradient along the height, *Fluid Dyn.*, 10, 745–750, 1976.
- Getling, A.V., Scales of convective flows in a horizontal layer with radiative transfer, *Izv., Atmosph. Oceanic Phys.*, 16, 363–365, 1980.
- Getling, A.V., *Rayleigh–Bénard Convection: Structures and Dynamics*, World Scientific, Singapore, 1998; URSS, Moscow, 1999.
- Getling, A.V., Do quasi-regular structures really exist in the solar photosphere? I. Observational evidence, *Solar Phys.*, 239, 93–111, 2006.
- Getling, A.V., Mazhorova, O.S., & Shcheritsa, O.V., Concerning the multiscale structure of solar convection, *Geomagn. Aeron.*, 53, 904–908, 2013.
- Getling, A.V., & Tikhomolov, E.M., Scale splitting in solar convection, *Trudy XI Pulkovskoi mezhdunarodnoi konferentsii po fizike Solntsa (Proc. 11th Pulkovo Int. Conf. on Solar Physics)*, Pulkovo, 2007, pp. 109–112.
- Kitiashvili, I.N., Kosovichev, A.G., Mansour, N.N., Lele, S.K., & Wray, A.A., Vortex tubes of turbulent solar convection, *Phys. Scr.*, 86, paper id. 018403, 2012.
- Kovenya, V.M., & Yanenko, N.N., *The Splitting Method in Problems of Gas Dynamics*, Novosibirsk, Nauka, 1981.
- Krishan, K., Kurtuldu, H., Schatz, M.F., Madruga, S., Gameiro, M., & Mischaikow, K., Homology and symmetry breaking in Rayleigh–Bénard convection: Experiments and simulations, *Phys. Fluids*, 19, 17105, 2007.
- Mazhorova, O.S., & Popov, Yu.P., Methods for the numerical solution of the Navier–Stokes equations, *USSR Comput. Math. Math. Phys.*, 20, 202–217, 1980.
- Mazhorova, O.S., & Popov, Yu.P., Matrix iteration method of numerical solution of Navier–Stokes two-dimensional equations, *Doklady Akad. Nauk SSSR*, 259, 535–540, 1981.
- November, L.J., Toomre, J., Gebbie, K.B. and Simon, G.W., The detection of mesogranulation on the Sun, *Astrophys. J. Lett.*, 245, L123–L126, 1981.
- Rogers, T.M., Glatzmaier, G.A., & Woosley, S.E., Simulations of two-dimensional turbulent convection in a density-stratified fluid, *Phys. Rev. E*, 67, article id. 026315, 2003.
- Schmalzl, J., Breuer, M., & Hansen, U., On the validity of two-dimensional numerical approaches to time-dependent thermal convection, *Europhys. Lett.*, 67, 390–396, 2004.
- Simon, G.W., & Leighton, R.B., Velocity fields in the solar atmosphere. III. large-scale motions, the chromospheric network, and magnetic fields, *Astrophys. J.*, 140, 1120–1147, 1964.
- Stengel, K.C., Oliver, D.S., & Booker, J.R., Onset of convection in a variable-viscosity fluid, *J. Fluid Mech.*, 120, 411–431, 1982.